Lawrence Berkeley National Laboratory
LBL Publications

Title

FATIGUE CRACK PROPAGATION IN ALUMINUM-LITHIUM ALLOY 2090: PART I. LONG CRACK BEHAVIOR

Permalink

https://escholarship.org/uc/item/6q70h0p4

Authors

Rao, K.T. Venkateswara
Yu, W.
Ritchie, R.O.

Publication Date

1986-11-01

eScholarship.org Powered by the California Digital Library
University of California

LBL-22178
Preprint

Lawrence Berkeley Laboratory
UNIVERSITY OF CALIFORNIA

Materials & Chemical Sciences Division

RECEIVED
APR 22 1987
DOCUMENTS SECTION

Center for Advanced Materials

Submitted to Metallurgical Transactions A

FATIGUE CRACK PROPAGATION IN ALUMINUM-LITHIUM ALLOY 2090: PART I. LONG CRACK BEHAVIOR

K.T. Venkateswara Rao, W. Yu, and R.O. Ritchie

November 1986

TWO-WEEK LOAN COPY
This is a Library Circulating Copy
which may be borrowed for two weeks.

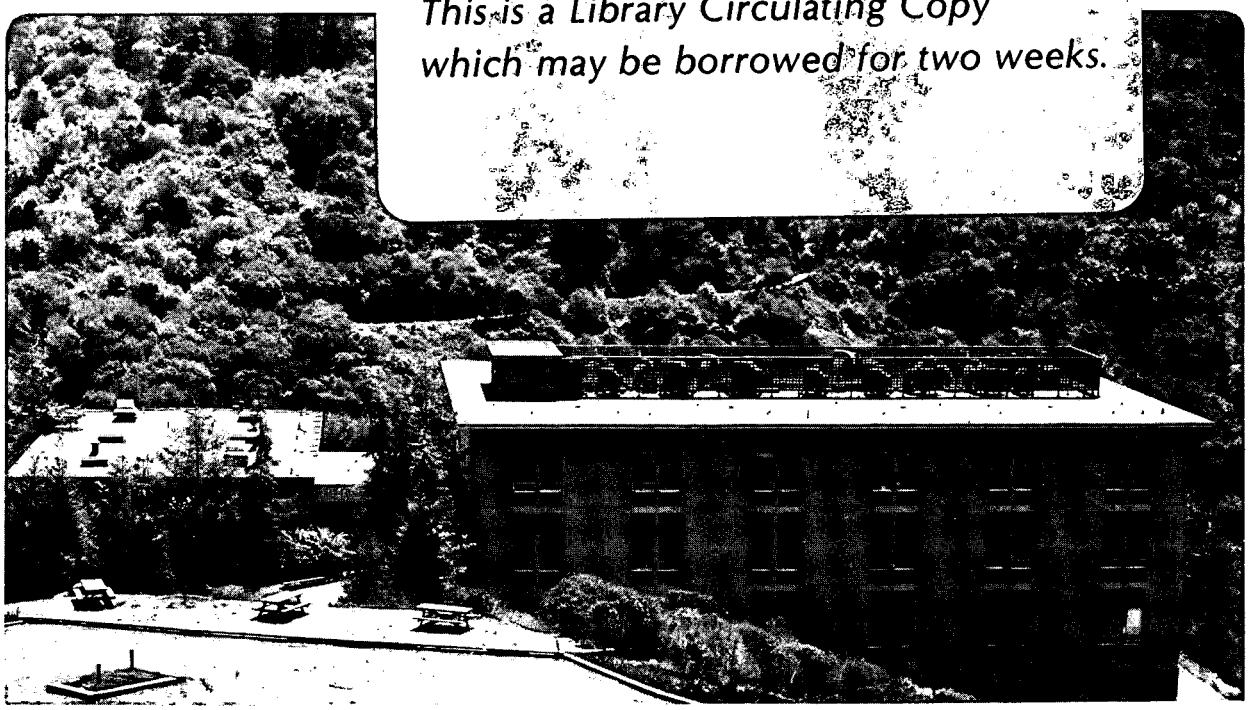

Prepared for the U.S. Department of Energy under Contract DE-AC03-76SF00098

LBL-22178

DISCLAIMER

This document was prepared as an account of work sponsored by the United States Government. While this document is believed to contain correct information, neither the United States Government nor any agency thereof, nor the Regents of the University of California, nor any of their employees, makes any warranty, express or implied, or assumes any legal responsibility for the accuracy, completeness, or usefulness of any information, apparatus, product, or process disclosed, or represents that its use would not infringe privately owned rights. Reference herein to any specific commercial product, process, or service by its trade name, trademark, manufacturer, or otherwise, does not necessarily constitute or imply its endorsement, recommendation, or favoring by the United States Government or any agency thereof, or the Regents of the University of California. The views and opinions of authors expressed herein do not necessarily state or reflect those of the United States Government or any agency thereof or the Regents of the University of California.

LBL-22178

FATIGUE CRACK PROPAGATION IN ALUMINUM-LITHIUM ALLOY 2090:

PART I. LONG CRACK BEHAVIOR

K. T. Venkateswara Rao, W. Yu and R. O. Ritchie

Center for Advanced Materials, Lawrence Berkeley Laboratory, and
Department of Materials Science and Mineral Engineering,
University of California, Berkeley CA 94720

November 1986

submitted to Metallurgical Transactions A

This work was supported by the Director, Office of Energy Research, Office of Basis Energy Sciences, Materials Sciences Division of the U.S. Departement of Energy under Contract No. DE-AC03-76SF00098.

FATIGUE CRACK PROPAGATION IN ALUMINUM-LITHIUM ALLOY 2090:

PART I: LONG CRACK BEHAVIOR

K. T. Venkateswara Rao, W. Yu, and R. O. Ritchie

Center for Advanced Materials, Lawrence Berkeley Laboratory, and
Department of Materials Science and Mineral Engineering,
University of California, Berkeley, CA 94720

ABSTRACT

A study has been made of the mechanics and mechanisms of fatigue crack propagation in a commercial plate of aluminum-lithium alloy 2090-T8E41. In Part I, the crack growth and crack shielding behavior of long ($\gtrsim$5 mm) through-thickness cracks is examined as a function of plate orientation and load ratio, and results compared to traditional high strength aluminum alloys. It is shown that rates of fatigue crack extension in 2090 are, in general, significantly slower (at a given stress intensity range) than in traditional alloys, although behavior is strongly anisotropic. Differences in growth rates of up to 4 orders of magnitude are observed between the L-T, T-L and T-S orientations, which show the best crack growth resistance, and the S-L, S-T and L+45, which show the worst. Such behavior is attributed to the development of significant crack tip shielding (i.e., a reduction in **local** crack driving force), primarily resulting from the role of the crack path morphology in inducing crack deflection and crack closure from the consequent asperity wedging. Whereas crack advance perpendicular to the rolling plane (e.g., L-T, etc.) involves marked crack path deflection and branching, thereby promoting very high levels of shielding to cause the slowest growth rates, fatigue fractures parallel to the rolling plane (e.g., S-L, etc.) occur by an intergranular, delamination-type separation, with much lower shielding levels to give the fastest growth rates. The implications of such "extrinsic toughening" effects on the fracture and fatigue properties of aluminum-lithium alloys are discussed in detail.

K. T. VENKATESWARA RAO, W. YU and R. O. RITCHIE are Graduate Student, Research Engineer and Professor, respectively, with the Center for Advanced Materials, Lawrence Berkeley Laboratory, and the Department of Materials Science and Mineral Engineering, University of California, Berkeley, CA 94720.

I. INTRODUCTION

Over the past few years, there has been increasing interest in the development of ultra-light weight aluminum-lithium alloys, specifically for aerospace structures (1-3) and, more recently, for cryogenic applications (4). The motivation for using such materials is primarily their 7-10 pct lower density, although compared to traditional high strength aluminum alloys, Al-Li-X alloys additionally show 7-12 pct higher stiffness, generally superior fatigue crack propagation resistance (4-12), and improved toughness at cryogenic temperatures (4,13). On the negative side, however, they can suffer from poor short-transverse properties, low ductility and fracture toughness (13,14), and have been shown to display significantly accelerated fatigue crack extension rates when cracks are microstructurally-small (15).

The low ductility and toughness of aluminum-lithium alloys can be traced, at least in part, to the inhomogeneous nature of their slip, resulting from coherent particle hardening of spherical δ' (Al_3Li) precipitates (16). In addition, the presence of equilibrium δ (AlLi) precipitates in grain boundaries can cause precipitate free zones, which can induce further strain localization and promote intergranular failure. Consequently, for the development of commercial alloys, slip has been homogenized by introducing dispersoids (Mn, Zr) and semi-coherent/incoherent precipitates, such as $T_1'(Al_2CuLi)$, $T_2'(Al_5CuLi_3)$ or Al_2LiMg, through Cu or Mg additions

(17). Concurrent developments in the thermomechanical processing have optimized aluminum-lithium microstructures for the best combinations of strength and toughness, although the resulting material tends to be highly textured, particularly where small Zr additions are used to inhibit recrystallization (18).

Although most studies on aluminum-lithium alloys to date have reported generally improved fatigue resistance compared to traditional 2000- and 7000-series alloys (4-12), due to their marked anisotropy, some concern has been raised over their crack propagation resistance as a function of plate orientation, and specifically with regard to short-transverse properties (i.e., involving crack propagation in the rolling plane). Accordingly, the objective of the current study is to investigate the mechanics and mechanisms of fatigue crack propagation behavior in an Al-Li-Cu-Zr alloy 2090-T8E41 as a function of orientation. In Part I, the behavior of through-thickness long ($\geq$ 5 mm) cracks is examined in the L-T, T-L, T-S, S-L, S-T and L+45 orientations, as a function of load ratio, with specific emphasis on the role of crack tip shielding* in

*Crack tip shielding refers to a phenomenon where crack advance is impeded through a **local** reduction in the "crack driving force" (extrinsic toughening), as distinct from an increase in the microstructural crack growth resistance (intrinsic toughening) (19,20). It can be developed from such mechanisms as transformation and microcrack toughening in ceramics (22) and crack closure during fatigue crack growth (20,22).

retarding crack growth. In Part II (23), such long crack behavior is compared with that for naturally-occurring microstructurally-small (2 to 1000 μm) surface cracks, in the L-T, T-L and T-S orientations. It is shown that, due to significant shielding from crack closure and deflection, long fatigue crack growth properties for 2090 compare favorably with 2124 and 7150 alloys of comparable strength. However, at equivalent stress intensity ranges, the growth rates of small cracks (where the limited wake inhibits shielding) are found to be accelerated significantly, typically by three orders of magnitude at near-thresholds levels.

II. EXPERIMENTAL PROCEDURES

A 12.7 mm thick plate of commercial Al-Li-Cu-Zr alloy 2090, of composition shown in Table I, was received from ALCOA in the near peak-aged T8E41 condition. The designation T8E41 refers to a thermomechanical treatment, involving solution treatment at 549°C, water quenching, and a 6 pct stretch prior to aging 24 h at 163°C (18).

Table I. Composition in Wt Pct of ALCOA Alloy 2090

Cu	Li	Zr	Fe	Si	Mg	Mn	Ti	Al
2.86	2.05	0.12	0.02	0.01	0.01	0.005	0.02	balance

Optical metallography revealed a highly unrecrystallized and anisotropic microstructure (Fig. 1), with large pan-cake shaped grains (approximately 20 μm thick and 500 μm wide), elongated for several mm along the rolling direction. In the peak aged T8 condition, the alloy is hardened by a combination of coherent precipitates, including spherical δ' (Al_3Li), plate-like T_1' (Al_2CuLi) and T_2' (Al_5CuLi_3), with β' (Al_3Zr) dispersoids (Fig. 2). Room temperature mechanical properties are listed in Table II, and indicate marked differences in the strength, ductility and toughness between the various orientations.

Table II. Room Temperature Mechanical Properties of 2090-T8E41

Orientation	Yield Strength	UTS	Elongation (14 mm gauge)	K_{Ic}
	(MPa)	(MPa)	(pct)	(MPa$\sqrt{m}$)
Longitudinal	552	589	9.3	35 (L-T)
Transverse	548	579	5.4	24 (T-L) 27 (T-S)
Short-Transverse	-	-	-	17 (S-L) 16 (S-T)
Longitudinal + 45°	460	514	10.9	28 (L+45)

Crack growth tests on long ($\gtrsim$ 5 mm) through-thickness cracks were performed with 6 to 7 mm thick test pieces, using compact C(T) specimens in the L-T, T-L and L+45 (LT-TL) orientations, double-cantilever beam DC(B) specimens in the S-L and S-T orientations, and four-point single-edge-notched bend SEN(B) specimens in the T-S

orientation (Fig. 3). Tests were conducted in controlled room temperature air (22°C, 45 pct relative humidity), using automated electro-servo-hydraulic testing machines operating under stress intensity control at a sinusoidal frequency of 50 Hz, over a range of load ratios ($R = K_{min}/K_{max}$) from 0.1 to 0.75. Fatigue threshold stress intensity ranges (ΔK_{TH}), defined at a maximum growth rate of 10^{-11} m/cycle, were approached using both manual and computer-controlled load-shedding procedures (normalized K-gradient set at -0.1 mm^{-1}), with crack lengths continuously monitored using d.c. electrical potential methods. Simultaneous measurement of crack closure was achieved using the back-face strain gauges on the C(T) and SEN(B) samples, and the crack mouth opening displacement gauges on the DC(B) samples. Using these techniques, the closure stress intensity (K_{cl}) was defined during unloading at first contact of the fracture surfaces from the load corresponding to the initial deviation from linearity of the elastic compliance curve (20). Crack growth rate (da/dN) data are presented in terms of the nominal stress intensity range ($\Delta K = K_{max} - K_{min}$), and the effective stress intensity range, defined as $\Delta K_{eff} = K_{max} - K_{cl}$.

Fatigue fracture surfaces were examined in the scanning electron microscope and from crack path profiles, obtained by metallographic sectioning at the specimen center thickness, perpendicular to the fracture surface, on cracks previously impregnated with epoxy. The degree of (lineal) fracture surface roughness was evaluated from such profiles in terms of the ratio of total length of crack to projected

length along the plane of maximum tensile stress. The extent of (excess) crack surface corrosion deposits was estimated by scanning Auger spectroscopy, using a tantalum oxide standard and an Ar^+ sputtering rate of 25 nm/min.

III. RESULTS

A. Crack Growth Rate and Closure Behavior

A comparison of fatigue crack propagation rates (da/dN) of long cracks in 2090-T8E41 (T-L orientation) with those of traditional high strength aluminum alloys, 2124 and 7150 (20,24), is shown in Fig. 4 as a function of the nominal stress intensity range (ΔK). Despite having 30 pct higher strength, long crack growth rates in the aluminum-lithium alloy are consistently slower over the entire range of growth rates, except at near-threshold levels in 2124-T351. As reported previously (12), such behavior can be attributed primarily to high levels of crack closure, which unlike other high strength aluminum alloys are maintained at almost near-threshold levels up to ΔK values of 7 MPa$\sqrt{m}$ and above (Fig. 5).

Role of Orientation: Despite its slower growth rates, crack propagation behavior in 2090 is strongly anisotropic, as shown in Fig. 6 for the L-T, T-L, T-S, S-L, S-T, and L+45 orientations tested at R = 0.1. This plot indicates variations in growth rates (at fixed ΔK) by up to 4 orders of magnitude between the various orientations,

consistent with large changes in crack closure (Fig. 7). The more commonly tested T-L and L-T orientations, and the T-S orientation, show the slowest growth rates, with threshold ΔK_{TH} values between 3 and 4 MPa$\sqrt{m}$. These orientations generally develop the highest closure levels, e.g., K_{cl} values approach 0.9 K_{max} close to ΔK_{TH} in the L-T orientation. Conversely, S-L and S-T show the fastest growth rates, consistent with the smallest extent of crack closure. The lowest threshold (ΔK_{TH} = 2.4 MPa$\sqrt{m}$) is found in the L+45 orientation, which has 16 pct lower yield strength.

Role of Load Ratio: Corresponding crack growth behavior at higher load ratios, specifically for R = 0.1, 0.5 and 0.75, are shown for the L-T, T-L, T-S and L+45 orientations in Fig. 8. Corresponding K_{cl} data are given in Fig. 9. Characteristic of most metallic materials (25), the role of load ratio is most prominent at near-threshold levels where ΔK_{TH} values are sharply decreased with increasing R. Such behavior is generally consistent with a diminished effect of closure at high load ratios, specifically from crack wedging mechanisms (20). In fact, by plotting the growth rate data in terms of ΔK_{eff} (after allowing for closure), the variation in da/dN with load ratio is much reduced (Fig. 8).

B. Fractography and Crack Path Morphology

Scanning electron micrographs of the fatigue fracture surfaces (at R = 0.1) are shown in Fig. 10 for the L-T, T-L, T-S, L+45, S-L

and S-T orientations. Although imaged at intermediate stress intensity ranges, i.e., at ΔK levels between 5 and 10 MPa$\sqrt{m}$, such surfaces were generally typical of the entire range of growth rates at all load ratios. Corresponding crack path profiles are shown in Fig. 11. For the L-T and T-L orientations, where growth rates were slowest, crack paths were relatively planar but showed evidence of local slip-band cracking on the scale of the grain size (Fig. 11a,b). This resulted in a faceted fracture surface morphology with alternating rough and smooth bands parallel to the crack growth direction (Fig. 10a,b), characteristic of coherent-particle hardened (planar slip) materials (24,26,27). Similar fractographic features were apparent for the T-S orientation, only now perpendicular to the crack growth direction (Fig. 10c), consistent with the boundaries between the facets being grain boundaries (c.f., Fig. 1). However, in this orientation, there was evidence of marked crack deviation and branching, and at longer crack lengths the crack underwent a major ($\sim 90^{o}$) deflection (**parallel** to the tensile stress axis) to follow an intergranular, delamination-type failure along the rolling plane (Fig. 11d). Such major deflections occurred in this orientation for all load ratios (Fig. 12). Delamination-type separation parallel to the rolling plane was also characteristic of the S-L and S-T orientations (Fig. 11e,f), where fracture surfaces were predominantly intergranular, smooth and featureless (Fig. 10e,f), and growth rates were correspondingly the fastest.

Fatigue fracture surfaces in all orientations showed evidence of slight abrasion and corrosion debris, resulting from asperity contact and fretting oxidation mechanisms. The oxide deposits were not continuous but were dispersed over the entire fracture surface. Excess oxide film thicknesses, deduced by Auger spectroscopy (28) in the T-L orientation, were found to be small (by one to two orders of magnitude) compared to computed crack tip opening displacements (Table III), i.e., less than 2 nm thick at all growth rates for R = 0.1-0.75 (Fig. 13), indicating that the contribution to crack tip shielding from oxide-induced crack closure (28,30-32) was relatively minor in this alloy. Conversely, contributions from crack deflection (33) and roughness-induced closure from asperity wedging (34-36) appeared to be far more significant, in light of the very high lineal roughnesses and mean angular deviations characteristic of fatigue fracture surfaces in the L-T, T-L, and T-S orientations of this alloy (Table III). The variation in lineal roughness with ΔK for the T-L orientation is shown in Fig. 13; mean values for each orientation are listed in Table III. It is clear that crack deflection and the resulting roughness-induced crack closure from the wedging of enlarged fracture surface asperities provide the principal mechanisms of crack tip shielding in this alloy.

Table III. Crack Path Morphology Measurements in 2090-T8E41 at R = 0.1

Orientation	Threshold ΔK_{TH}	Threshold ΔK_{eff}	CTOD* max	CTOD* cyclic	Lineal Roughness	Mean Angular Deviation	Excess Oxide Thickness
	($MPa\sqrt{m}$)		(nm)			(deg)	(nm)
L-T	3.86	0.84	255	103	1.23	20.4	-
T-L	3.21	0.97	177	72	1.26	17.3	2
T-S	3.06	0.97	162	65	1.83	39.2	-
S-L	2.60	1.36	117	47	1.11	3.6	-
S-T	2.75	1.09	130	53	1.11	4.5	-
L+45	2.46	0.71	124	50	1.09	5.8	-

*Maximum and cyclic CTOD computed from $0.6\ K^2_{max}/\sigma_o E$ and $0.6\ \Delta K^2/2\sigma_o E$, respectively, where E is Young's modulus and σ_o is the yield strength (29).

IV. DISCUSSION

There is now general accord that the fatigue crack propagation resistance of aluminum-lithium alloys is generally superior to traditional high strength aluminum alloys* (1-12). Several reasons have been advanced for this, including their higher elastic modulus (induced by δ' (Al_3Li) precipitation), which reduces the crack tip opening displacement at a given stress intensity (5), their

*It is important to note that this conclusion applies strictly to the behavior of long cracks, of a size large compared to the relevant dimensions of microstructure and local plasticity (15). Where cracks are microstructurally-small, aluminum-lithium alloys show anomalously high crack growth rates, as discussed in Part II of this paper (23).

planar slip characteristics (also induced by ordered δ' precipitation), which enhances slip-reversibility (and hence creates less "damage") at the crack tip (5,6,9), and the tortuous nature of the crack path, which promotes crack tip shielding via crack deflection and closure mechanisms (7,9-12). Whereas all three mechanisms undoubtedly act in concert to various degrees, in view of the high measured levels of closure and deflection, the large load ratio dependence of near-threshold growth rates, and the anomalously high small crack effects (15,23), it would now appear that enhanced shielding is the prominent factor for the excellent fatigue crack growth properties of these alloys (see also refs. 7,9-12).

The prominent mechanisms of shielding in the 2090 alloy have been shown to be associated with crack branching and deflection, which induce a multiplicative reduction in **local** stress intensity at the crack tip, and roughness-induced crack closure, where the wedging action of resulting enlarged fracture surface asperities acts to wedge the crack, thereby reducing the **local** stress intensity range by effectively raising K_{min} (Fig. 14). The latter wedge shielding mechanism predominates at low load ratios and low ΔK levels, where the size of the wedge becomes comparable with the crack opening displacements, whereas shielding by deflection may be expected to be independent of R and ΔK (provided the crack path morphology remains similar) (19,20). Contributions from other shielding mechanisms, such as closure arising from cyclic plasticity (37), cannot of course be dismissed, although the role of oxide-induced closure in these alloys

appears to be minimal in view of the small excess oxide thicknesses compared to crack tip opening displacements (Table III).

The precise mechanisms of roughness-induced crack closure in 2090 result from three types of crack deflection. As illustrated in Fig. 15, the marked planar slip characteristics of aluminum-lithium alloys induce crystallographic crack growth where crack advance proceeds along slip bands. This may be manifest as macroscopic crack branching, where the entire crack extends at some angle ($\sim 45^{o}$) to the plane of maximum stress, as shown by the L-T orientation in Fig. 15a, or more commonly as faceted crack growth, where the crack undergoes periodic "zig-zags" (on the scale of the grain size) but still grows primarily along the plane of maximum tensile stress, as shown by the L+45 orientation in Fig. 15b. A third type of (milder) crack deflection occurs in the S-L and S-T orientations, where linkage occurs between intergranular delamination cracks in the rolling plane (Fig. 15c).

It is apparent that the nature of the crack deflection has a critical influence on the anisotropy of crack growth rates. The fastest growth rates occur for crack advance in the rolling plane, i.e., in the short-transverse S-L and S-T orientations, where the unrecrystallized, elongated pancake-shaped grain structure provides a weak path along the grain boundaries. In this orientation, the degree of crack deflection and shielding is consequently the lowest (Figs. 7,15c). Conversely, in the longitudinal and transverse L-T, T-L, T-S orientations where general crack advance is perpendicular to the

weaker rolling plane, the slowest growth rates are observed as the crack encounters grain boundaries and undergoes crystallographic deflection and delamination perpendicular to the crack plane (Fig. 16). Behavior is thus analogous to an aligned composite, as the planes of weakness perpendicular to the short-transverse direction (i.e., in the rolling plane) actually promote beneficial crack growth properties (via shielding) perpendicular to these planes. **Accordingly, attempts at improving the short-transverse properties through refinements in processing and thermomechanical treatments etc. may actually compromise the superior fatigue and fracture properties in the other directions.**

The crystallographic crack path morphologies, shown by most orientations in the 2090-T8E41 alloy, are not uncommon in precipitation-hardened aluminum alloys, particularly at near-threshold levels in planar slip microstructures (24,26,27). Behavior in 2090, however, is striking in that this fracture mode persists to much higher growth rates, accounting for the higher levels of closure and the much slower growth rates compared to traditional aluminum alloys, particularly **above 10^{-9} m/cycle** (Figs. 4,5). For most aluminum alloys, the crystallographic fracture mode, and associated high closure levels, predominate only at low stress intensities, typically where the cyclic plastic zone size remains less than the order of the grain size (38).

Finally, the fatigue behavior of aluminum-lithium alloys provides a prime example of "extrinsic toughening", where superior

crack growth properties are achieved through microstructural, mechanical or environmental mechanisms which impede crack advance by **locally** reducing the "crack driving force", rather than by increasing the microstructural crack growth resistance (19,20). Although commonly employed to toughen brittle materials, e.g., by utilizing the transformation, microcrack or ligament toughening mechanisms in ceramics (19,21,39), the crack tip shielding approach is generally less applicable in metallic materials due to their high intrinsic toughness. The exception to this is where crack extension proceeds at low applied "driving forces", e.g., during sub-critical crack growth, where the effect can be extremely potent. However, it is important to note that the origins of shielding generally involve mechanisms that operate primarily **behind the crack tip**, rather than in the frontal zone. Such "wake effects" imply that crack extension rates will become strongly **crack-size dependent**, which has profound implications for fracture properties of materials which rely on extrinsic mechanisms.

First, extrinsically toughened materials will show marked resistance-curve fracture toughness behavior, as the "driving force" to sustain cracking must increase with increasing crack length (until steady-state). Such behavior has been recently reported for aluminum-lithium alloys (40).

Second, as shielding in 2090 depends largely on wedge mechanisms, where crack surface contact is diminished, i.e., at larger crack opening displacements or from a flattening of the

fracture surface, higher growth rates are to be expected. Consequently, aluminum-lithium alloys show large load ratio effects (Fig. 8), and are particularly sensitive to periodic compression overload cycles (12). In the latter case, the compressive loads act to reduce closure by crushing the smaller asperities, which can result in reduced closure, accelerated crack propagation rates and growth at the threshold (12).

Third, microstructural factors known to be beneficial for resistance to crack initiation may have a very different effect on the growth of long cracks. This follows because the role of shielding becomes negligible where the crack wake is small or non-existent. In 2090, however, this may be less of a problem as the higher strength of this alloy is generally beneficial for crack initiation resistance.

Finally, this same influence of minimal shielding with limited crack wake will result in small cracks seeing a higher local "driving force", compared to equivalent long cracks at the same ΔK (20,41). This is particularly significant in aluminum-lithium alloys because their superior long crack properties depend largely on extrinsic mechanisms (15). The anomalously high growth rate behavior of microstructurally-small cracks in 2090 alloy is discussed in Part II (23) of this paper.

V. CONCLUSIONS

Based on a study of the crack propagation and crack closure behavior of long (≥5 mm) fatigue cracks in 12.7 mm thick plate of commercial Al-Li-Cu-Zr alloy 2090-T8E41, the following conclusions can be made:

1. Rates of fatigue crack propagation in 2090 are found to be generally slower than in 2124 and 7150 aluminum alloys (over a wide range of da/dN from 10^{-12} to 10^{-6} m/cycle), despite having 30 pct higher strength. Such superior crack growth properties are associated with highly deflected and branched crack paths, which promote significant crack tip shielding from crack deflection and resulting crack closure due to the wedging of fracture surface asperities.

2. Fatigue crack growth rates in 2090, plotted as a function of the nominal stress intensity range ΔK, are strongly dependent upon load ratio, consistent with the high closure levels at low R. By plotting as a function of the effective stress intensity ΔK_{eff} (after correcting for closure), the load ratio dependence of growth rates is significantly diminished.

3. Fatigue crack growth and closure behavior in 2090 is found to be highly anisotropic, with growth rates varying by up to 4 orders between different orientations. The fastest growth rates, with associated lowest measured levels of closure, are observed where crack extension occurs perpendicular to the short-transverse

direction (in the rolling plane), e.g., in the S-L and S-T orientations. The slowest growth rates, with associated highest levels of closure, conversely are observed where crack extension is perpendicular to the rolling plane, e.g., in the L-T, T-L and T-S orientations.

4. The marked anisotropy in growth rate behavior is attributed to differences in crack tip shielding from crack deflection and closure, arising from differences in the morphology of the crack path. Due to the unrecrystallized, elongated grain structure perpendicular to the short-transverse direction, crack extension in the rolling plane (i.e., S-L, S-T) occurs by an intergranular delamination-type mechanism, with little associated shielding. Significant shielding, conversely, is developed for crack growth perpendicular to the rolling plane (i.e, T-L, T-S), where crack extension is primarily crystallographic with evidence of microscopic deflection and macroscopic branching.

ACKNOWLEDGEMENTS

This work was supported by the Director, Office of Energy Research, Office of Basic Energy Sciences, Materials Sciences Division of the U.S. Department of Energy under Contract No. DE-AC03-76SF00098, under the auspices of the Center for Advanced Materials. Thanks are due to Drs. P. E. Bretz, R. J. Bucci and R. R. Sawtell of ALCOA for supplying the 2090 plate, and to Drs. G. R. Chanani and G.

V. Scarich for providing additional alloy through the NAVAIR Collaborative Test Program. We also thank H. Hayashigatani and F. Haubensak for experimental assistance, and Ms. M. Penton for her help in preparing the manuscript. Several discussions with personnel at ALCOA, Boeing, Northrop, and Lockheed, and the research groups of Profs. J. W. Morris, G. Thomas and T. M. Devine at LBL, are also gratefully acknowledged.

REFERENCES

1. T. H. Sanders and E. A. Starke, eds.: "Aluminum-Lithium Alloys", Proc. First Intl. Conf., Stone Mountain, GA, TMS-AIME, Warrendale, PA, 1981.

2. T. H. Sanders and E. A. Starke, eds.: "Aluminum-Lithium Alloys II", Proc. Second Intl. Conf., Monterey, CA, TMS-AIME, Warrendale, PA, 1983.

3. C. Baker, P. J. Gregson, S. J. Harris, and C. J. Peel, eds.: "Aluminium-Lithium Alloys III", Proc. Third Intl. Conf., Oxford, U.K., Institute of Metals, London, U.K., 1986.

4. J. Glazer, S. L. Verzasconi, E. N. C. Dalder, W. Yu, R. A. Emigh, R. O. Ritchie, and J. W. Morris: Advances in Cryogenic Engineering, vol. 32, 1986, pp. 397-404.

5. E. J. Coyne, T. H. Sanders, and E. A. Starke: in ref. 1, pp. 293-305.

6. S. J. Harris, B. Noble, and K. Dinsdale: in ref. 2, pp. 219-33.

7. A. K. Vasudévan, P. E. Bretz, A. C. Miller, and S. Suresh: Mater. Sci. Eng., vol. 64, 1984, pp. 113-22.

8. G. R. Chanani, G. V. Scarich, and K. M. Bresnahan: in Mechanical Properties and Phase Transformations in Engineering Materials, S. D. Antolovich, R. O. Ritchie, and W. W. Gerberich, eds., TMS-AIME, Warrendale PA, 1986, pp. 271-91.

9. K. V. Jata and E. A. Starke: Metall. Trans. A, vol. 17A, 1986, pp. 1011-26.

10. J. Petit, S. Suresh, A. K. Vasudévan, and R. C. Malcolm: in ref. 3, pp. 257-62.

11. M. Peters, K. Welpmann, W. Zink, and T. H. Sanders: in ref. 3, pp. 239-46.

12. W. Yu and R. O. Ritchie: J. Eng. Matls. Tech., Trans. ASME, Series H, vol. 109, 1987.

13. R. C. Dorward: Scripta Met., vol. 20, 1986, pp. 1379-83.

14. D. Webster, G. Wald, and W. S. Cremens: Metall. Trans. A, vol. 12A, 1981, pp. 1495-502.

15. K. T. Venkateswara Rao, W. Yu, and R. O. Ritchie: Scripta Met., vol. 20, 1986, pp. 1459-64.

16. R. J. Rioja and E. A. Ludwiczak: in ref. 3, pp. 471-82.

17. M. H. Tosten, A. K. Vasudévan, and P. R. Howell: in ref. 3, pp. 483-9.

18. R. J. Rioja, P. E. Bretz, R. R. Sawtell, W. H. Hunt, and E. A. Ludwiczak: in Aluminum Alloys: Their Physical and Mechanical Properties, E. A. Starke and T. H. Sanders, eds., EMAS Ltd., Warley, U.K., 1986.

19. R. O. Ritchie and R. M. Cannon: "Crack Tip Shielding in Fracture and Fatigue: Extrinsic vs. Intrinsic Toughening", Lawrence Berkeley Laboratory Report No. LBL-20656, University of California, Berkeley, 1986.

20. R. O. Ritchie and W. Yu: in Small Fatigue Cracks, R. O. Ritchie and J. Lankford, eds., TMS-AIME, Warrendale, PA, 1986, pp. 167-89.

21. A. G. Evans and K. T. Faber: J. Amer. Cer. Soc., vol. 67, 1984, pp. 255-60.

22. S. Suresh and R. O. Ritchie, in Fatigue Crack Growth Threshold Concepts, D. L. Davidson and S. Suresh, eds., TMS-AIME, Warrendale, PA, 1984, pp. 227-61.

23. K. T. Venkateswara Rao, W. Yu, and R. O. Ritchie: Part II, submitted to Metall. Trans. A, vol. 18A, 1987.

24. E. Zaiken and R. O. Ritchie: Mater. Sci. Eng., vol. 70, 1985, pp. 151-60.

25. R. O. Ritchie: Intl. Metals Reviews, vol. 20, 1979, pp. 205-30.

26. S. Suresh, A. K. Vasudévan, and P. E. Bretz: Metall. Trans. A, vol. 15A, 1984, pp. 369-79.

27. R. D. Carter, E. W. Lee, E. A. Starke, and C. J. Beevers: ibid., pp. 555-63.

28. S. Suresh and R. O. Ritchie: Scripta Met., vol. 17, 1983, pp. 575-80.

29. C. F. Shih: J. Mech. Phys. Solids, vol. 29, 1981, pp. 305-30.

30. R. O. Ritchie, S. Suresh, and C. M. Moss: J. Eng. Matls. Tech., Trans. ASME, Series H, vol. 102, 1980, pp. 293-9.

31. A. T. Stewart: Eng. Fract. Mech., vol. 13, 1980, pp. 463-78.

32. S. Suresh, G. F. Zamiski, and R. O. Ritchie: Metall. Trans. A, vol. 12A, 1981, pp. 1435-43.

33. S. Suresh: ibid., vol. 14A, 1983, pp. 2375-85.

34. N. Walker and C. J. Beevers: Fat. Eng. Mat. Struct., vol. 1, 1979, pp. 135-48.

35. K. Minakawa and A. J. McEvily: Scripta Met., vol. 6, 1981, pp. 633-6.

36. S. Suresh and R. O. Ritchie: Metall. Trans. A, vol. 13A, 1982, pp. 1627-31.

37. W. Elber: Eng. Fract. Mech., vol. 2, 1970, pp. 37-45.

38. R. O. Ritchie and S. Suresh: Metall. Trans. A, vol. 13A, 1982, pp. 937-40.

39. D. B. Marshall, B. N. Cox, and A. G. Evans: Acta Met., vol. 11, 1985, pp. 2013-21.

40. S. Suresh and A. K. Vasudévan: Mater. Sci. Eng., vol. 79, 1986, pp. 183-90.

41. R. O. Ritchie and J. Lankford: ibid., vol. 84, 1986, pp. 11-6.

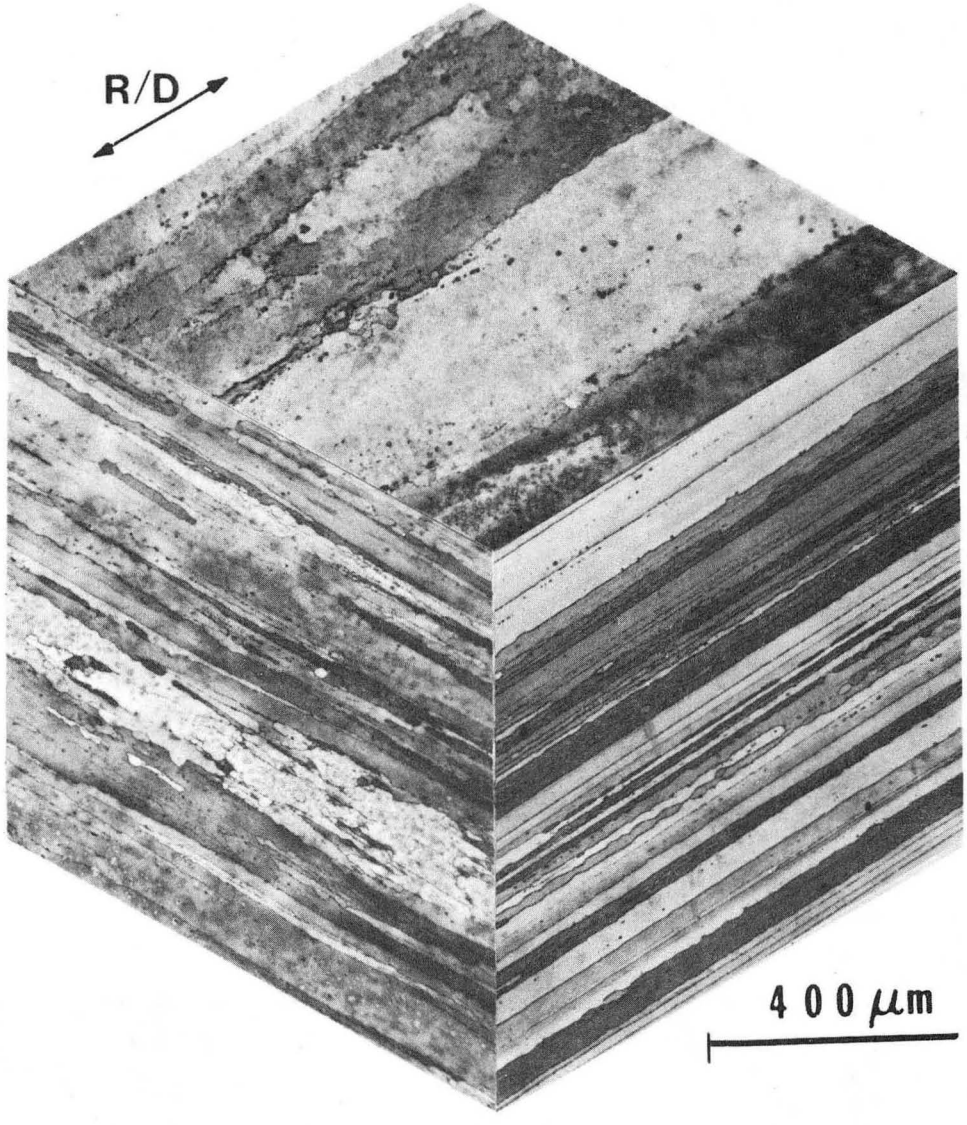

XBB 864-3075

Fig. 1: Optical microstructure of the three-dimensional grain structure 12.7 mm plate of commercial aluminum-lithium alloy 2090-T8E41 (Keller's reagent etch).

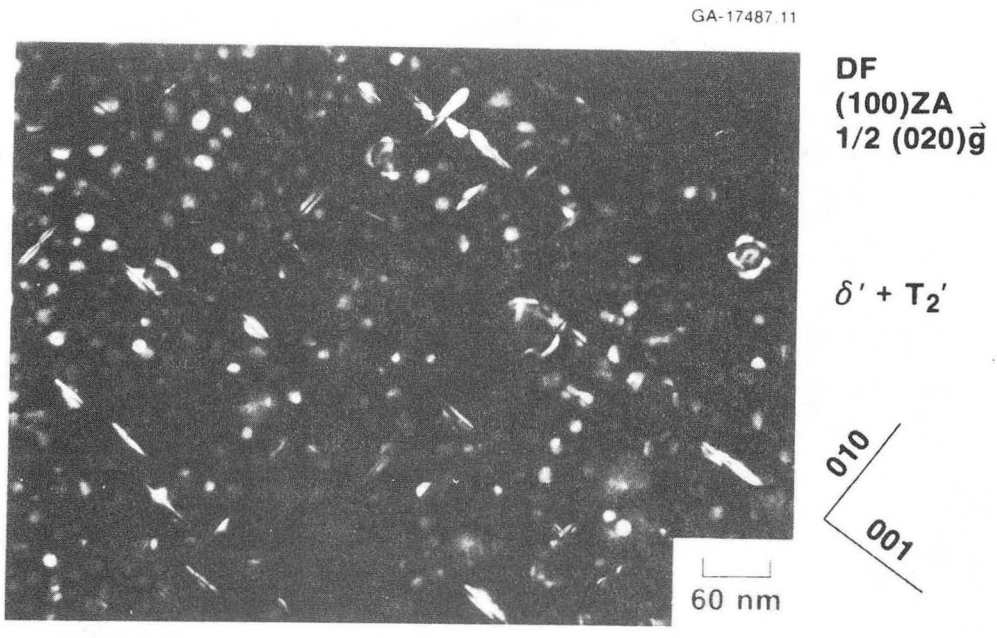

Fig. 2: Dark field transmission electron micrograph of the fine-scale microstructure of 2090-T8E41 alloy, showing heterogeneous precipitation of δ' on T_2' precipitates (courtesy of R. J. Rioja).

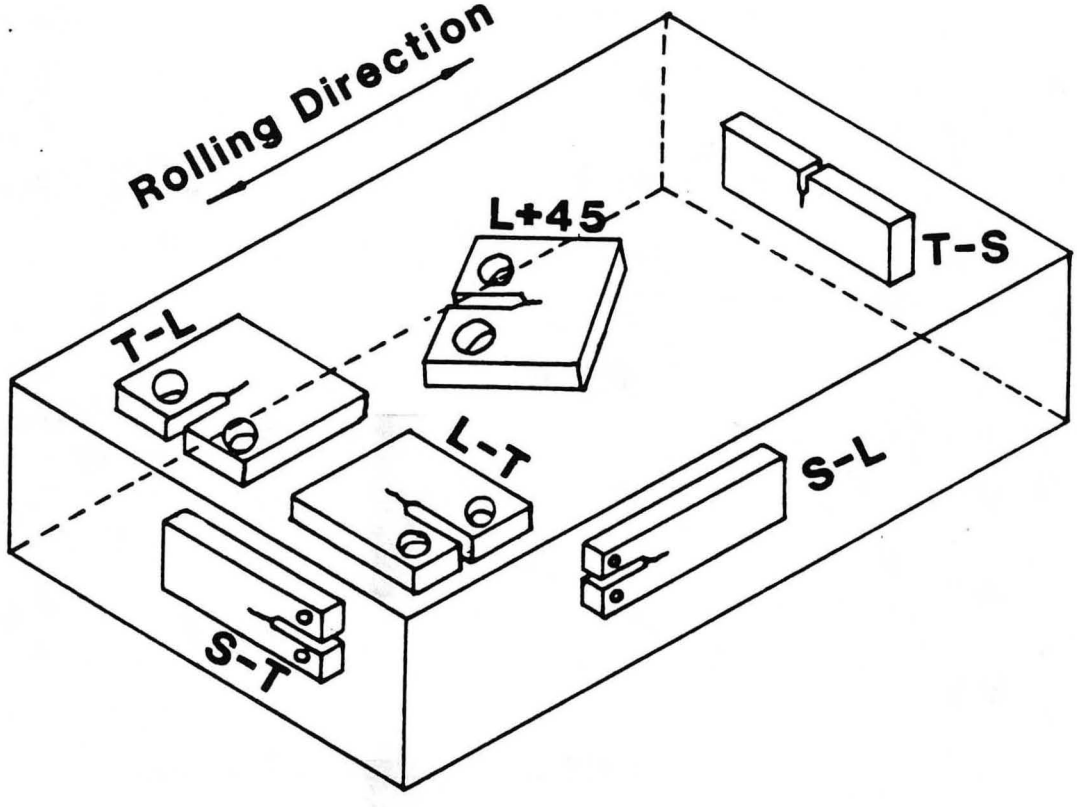

XBL 8610-3731

Fig. 3: Nomenclature relating to test specimen orientation and geometry relevant to long crack fatigue crack growth tests.

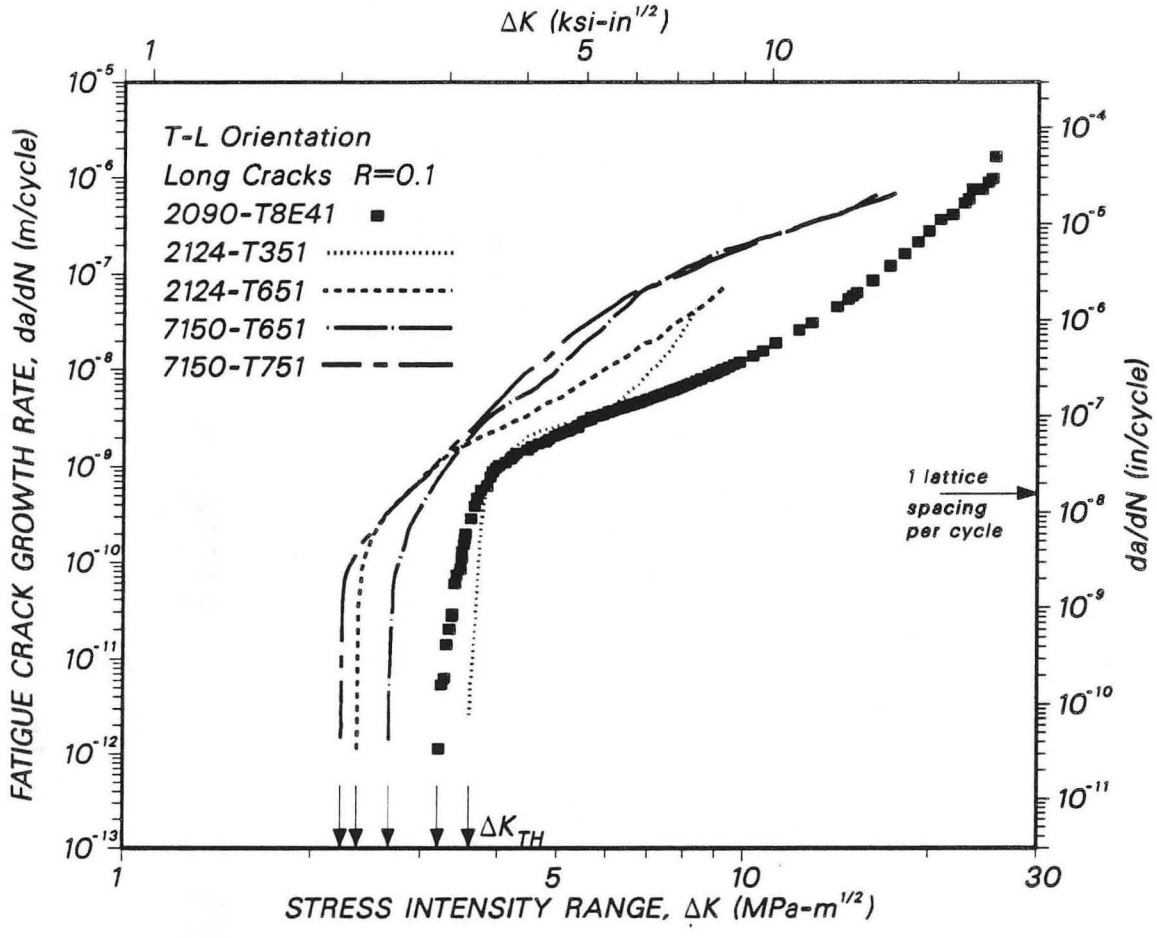

Fig. 4: Crack propagation behavior of long fatigue cracks in 2090-T8E41 (T-L orientation), as a function of the nominal stress intensity range ΔK, compared to corresponding results (20,24) in 2124 and 7150 alloys. Data for tests in moist air at R = 0.1.

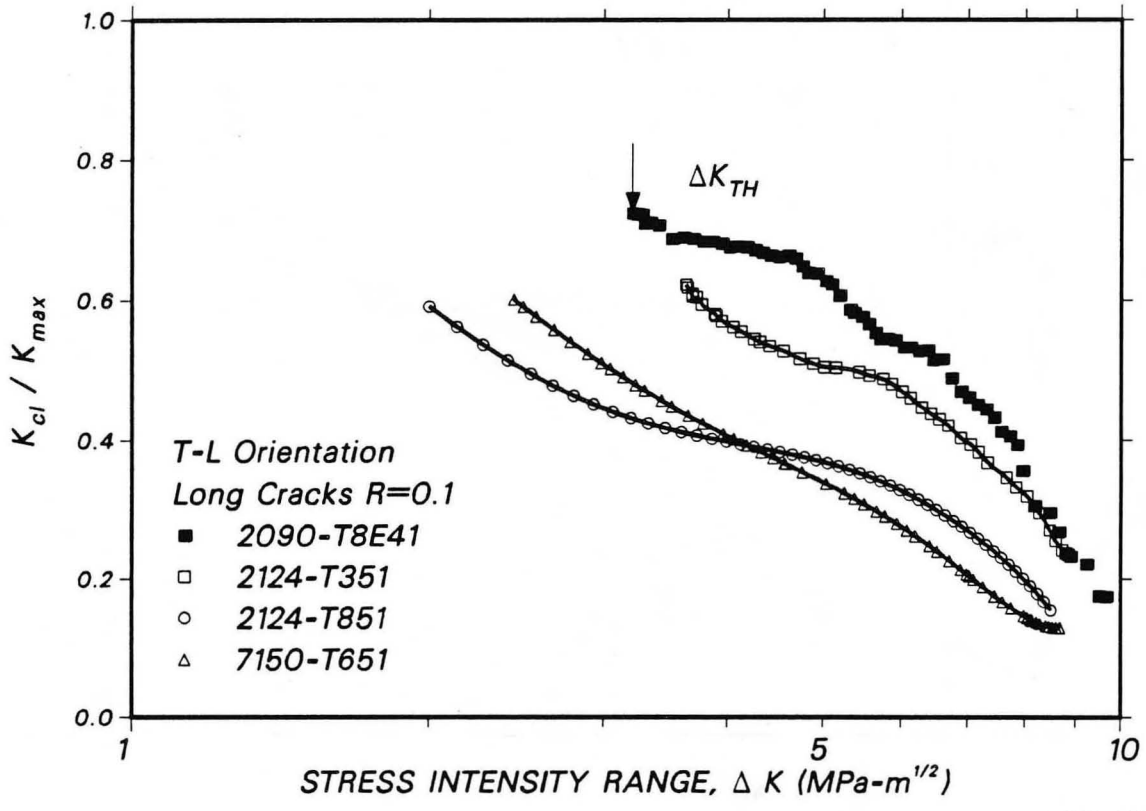

Fig. 5: Variation in crack closure stress intensity, K_{Cl}, normalized with respect to K_{max}, with nominal stress intensity range, ΔK, for 2090-T8E41 (T-L orientation) at R = 0.1. Data are relevant to the long crack growth results in Fig. 4, and indicate differences in closure levels between 2090 and traditional high strength alloys 2124 and 7150 (12,20,24).

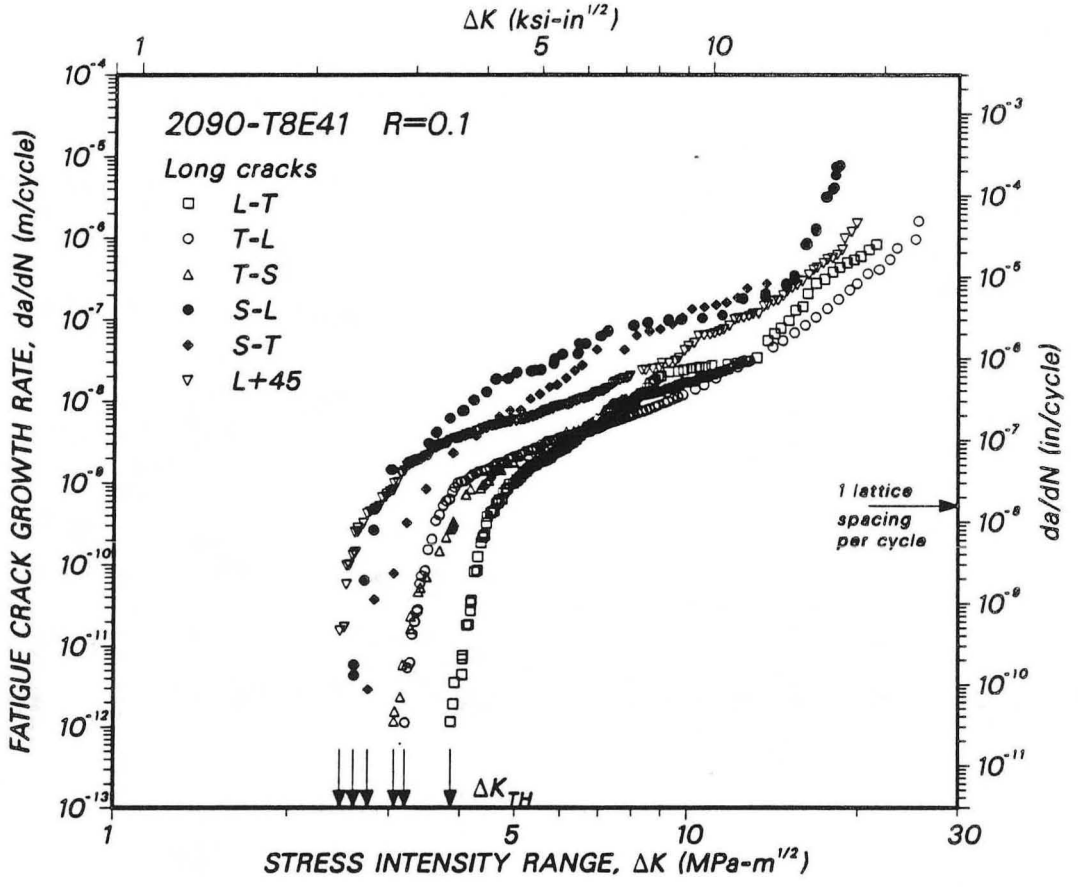

XBL 871-88

Fig. 6: Variation in fatigue crack growth rates (long cracks) in 2090-T8E41 alloy at R = 0.1 as a function of orientation. Note how growth rates parallel to the rolling plane (e.g., S-L, S-T) are generally the fastest, whereas growth rates perpendicular to the rolling plane (e.g., L-T, T-S) are the slowest. Growth rates are plotted in terms of the nominal stress intensity range, ΔK.

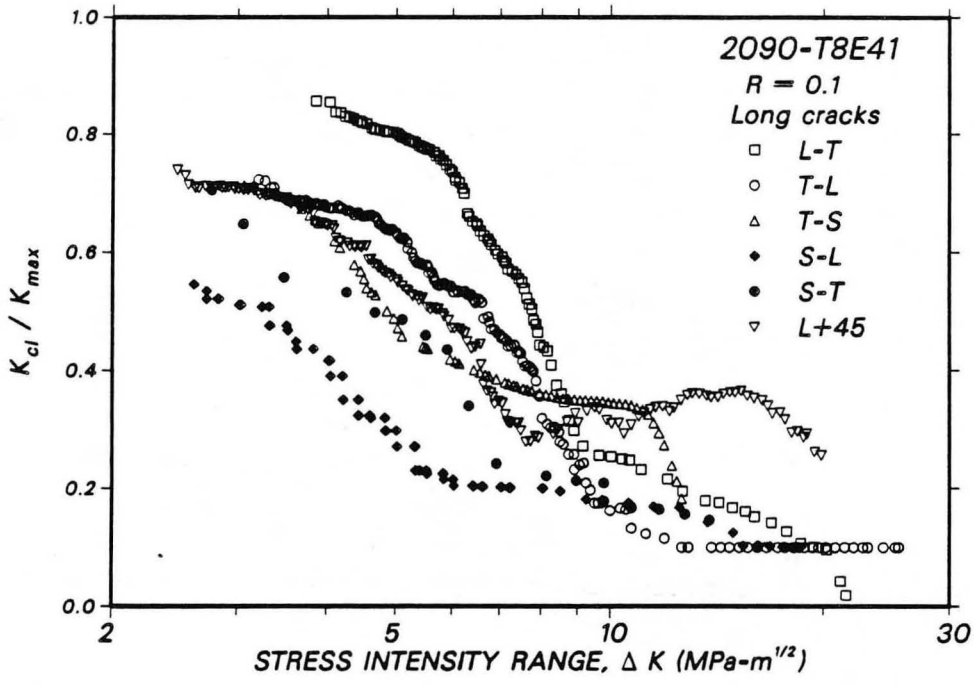

XBL 871-87

Fig. 7: Variation in closure stress intensity, K_{cl}, normalized with respect to K_{max}, with nominal stress intensity range, ΔK, for long cracks in 2090-T8E41 alloy (at R = 0.1) as a function of orientation. K_{cl} values are continuously monitored using back-face strain compliance techniques.

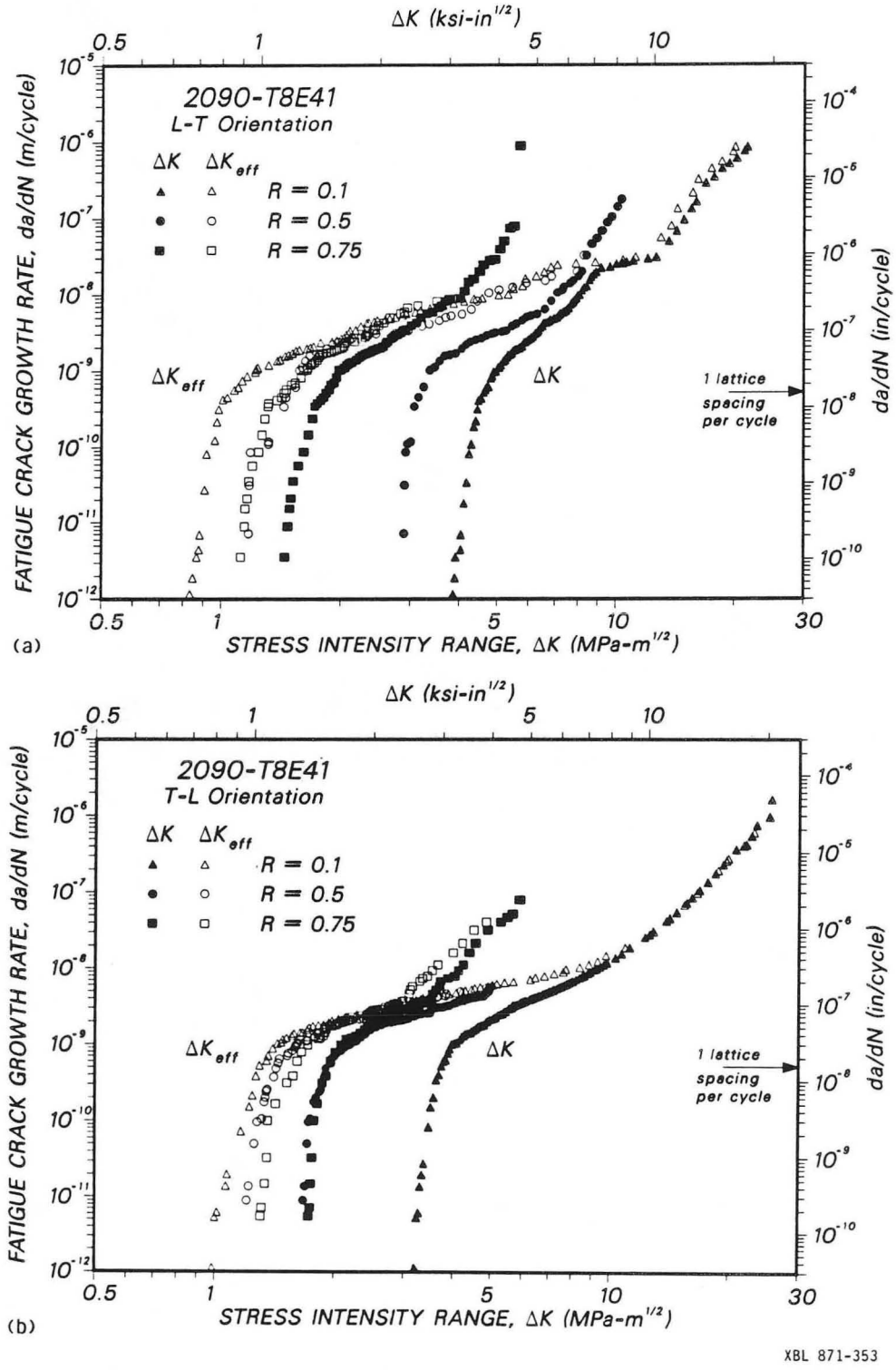

Fig. 8: Effect of load ratio R on the fatigue crack propagation behavior (long cracks) in 2090-T8E41 alloy, plotted as a function of both nominal and effective stress intensity ranges, ΔK and ΔK_{eff}, respectively, for a) L-T, b) T-L, c) T-S, and d) L+45 orientations.

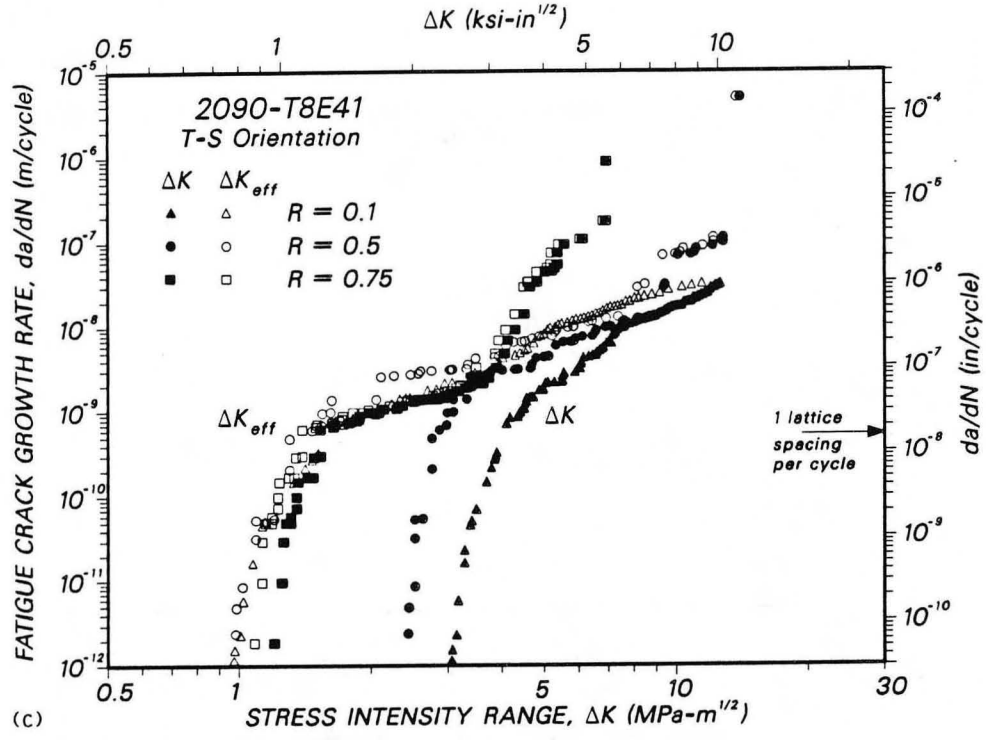

(c)

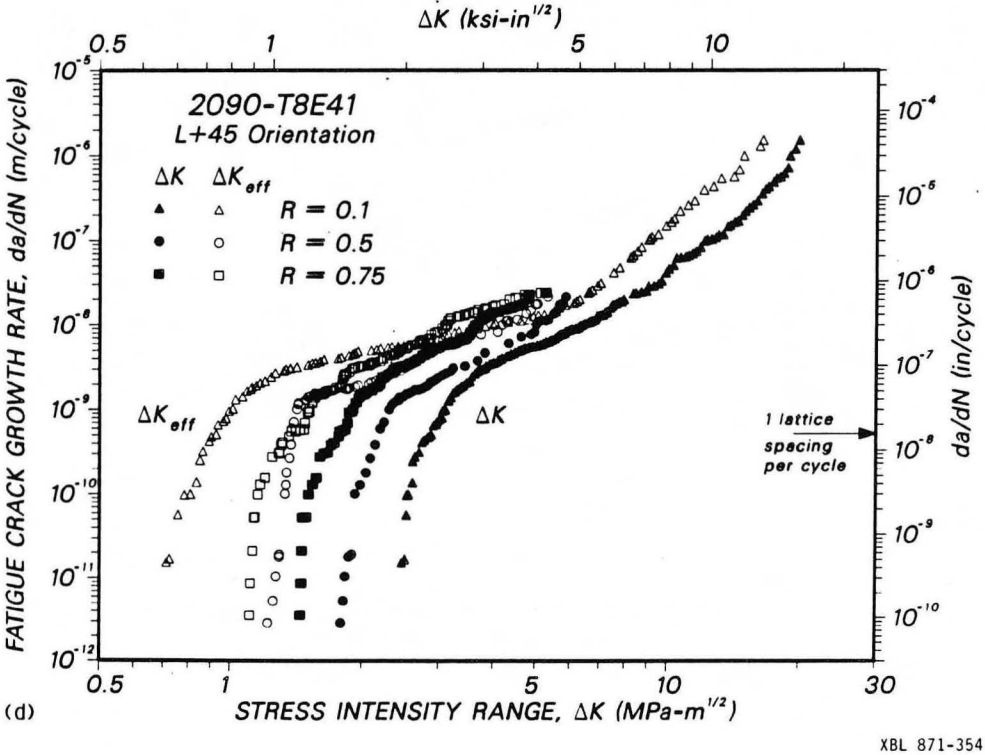

(d)

XBL 871-354

Fig. 8 (Cont.)

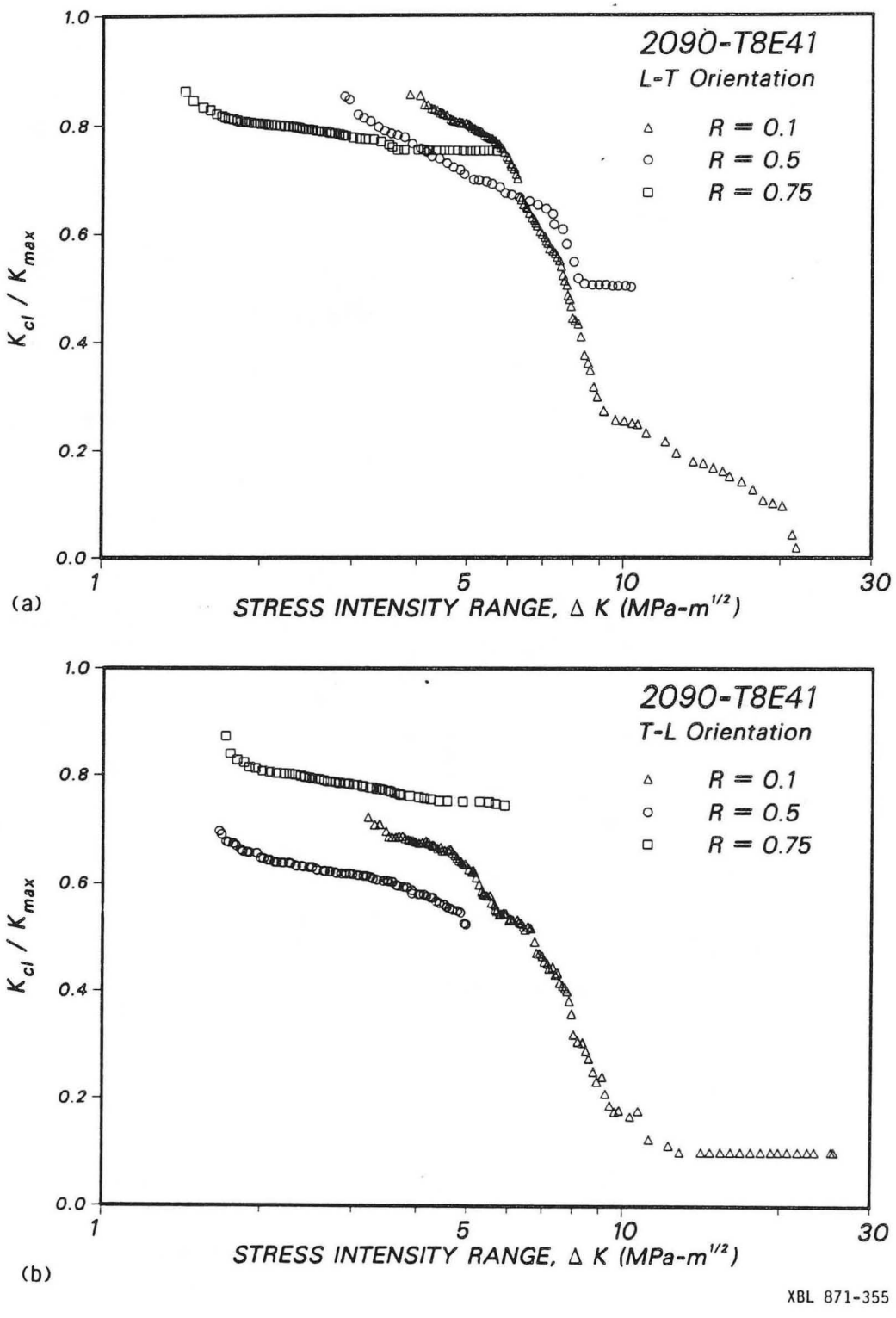

Fig. 9: Crack closure stress intensity K_{cl} data as a function of load ratio R for 2090-T8E41 alloy, corresponding to the crack growth data in Fig. 8. Back-face strain results are shown for a) L-T, b) T-L, c) T-S, and d) L+45 orientations.

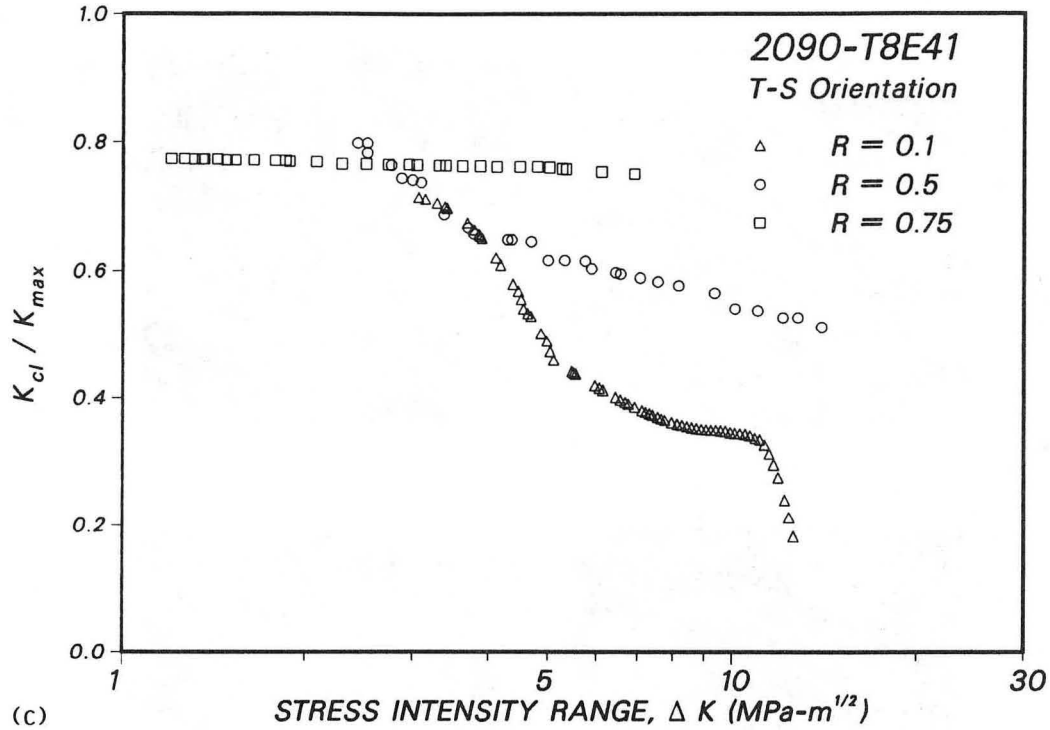

(c)

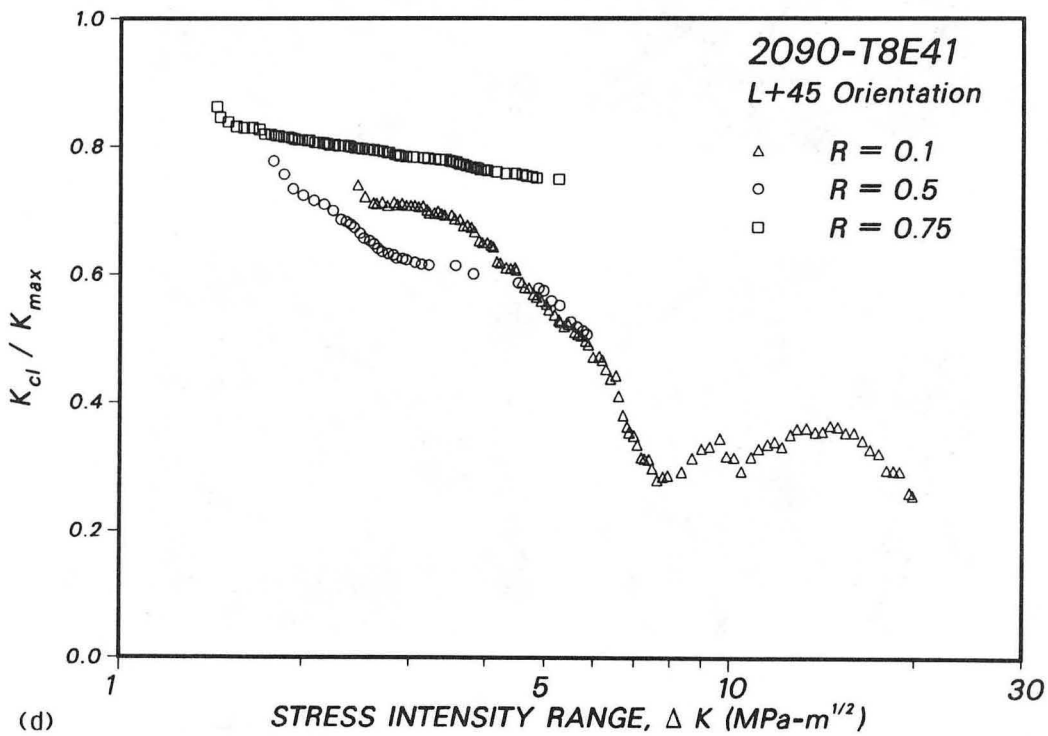

(d)

XBL 871-356

Fig. 9 (Cont.)

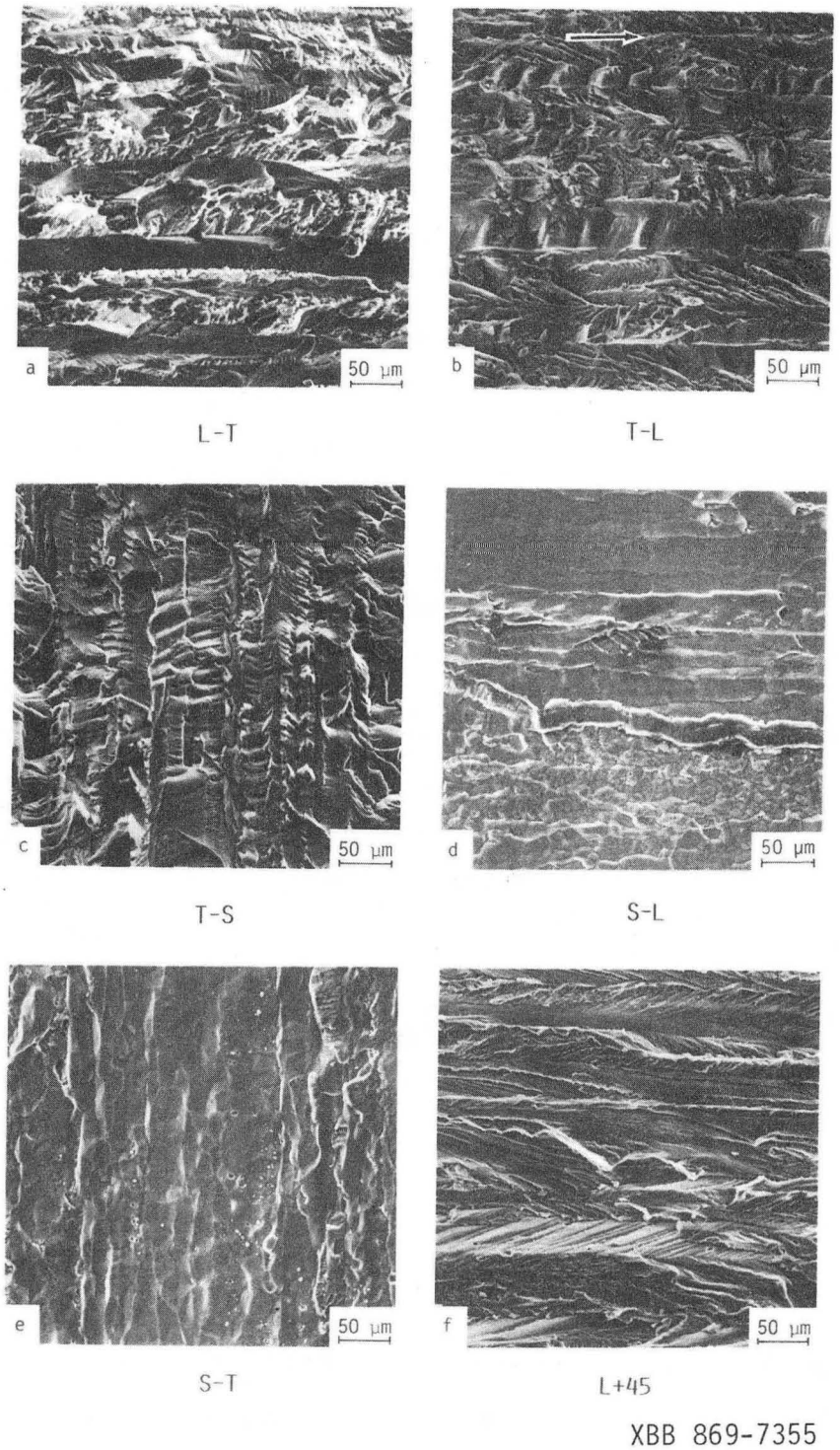

Fig. 10: Scanning electron micrographs of near-threshold fatigue fracture surfaces in 2090-T8E41 alloy, at ΔK levels between 3 and 8 MPa$\sqrt{m}$ ($R = 0.1$), for a) L-T, b) T-L, c) T-S, d) S-L, e) S-T, and f) L+45 orientations. Arrow indicates general direction of crack growth.

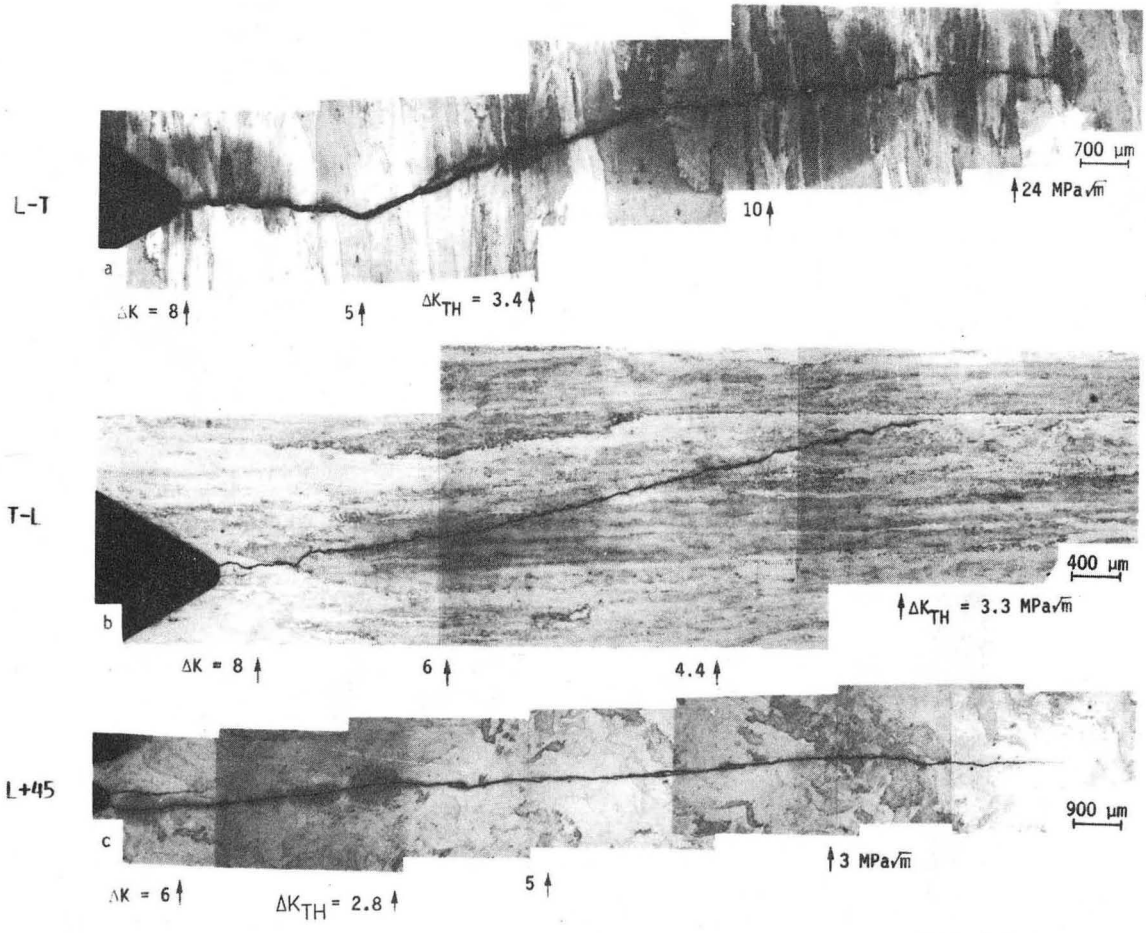

Fig. 11: Crack path morphology for long crack growth at R = 0.1 in 2090-T8E41 alloy in the a) L-T, b) T-L, c) L+45, d) T-S, e) S-L, and f) S-T orientations. The profiles, which are derived from metallographic sections taken perpendicular to the crack surface at the center of the specimen, are typical for all load ratios tested.

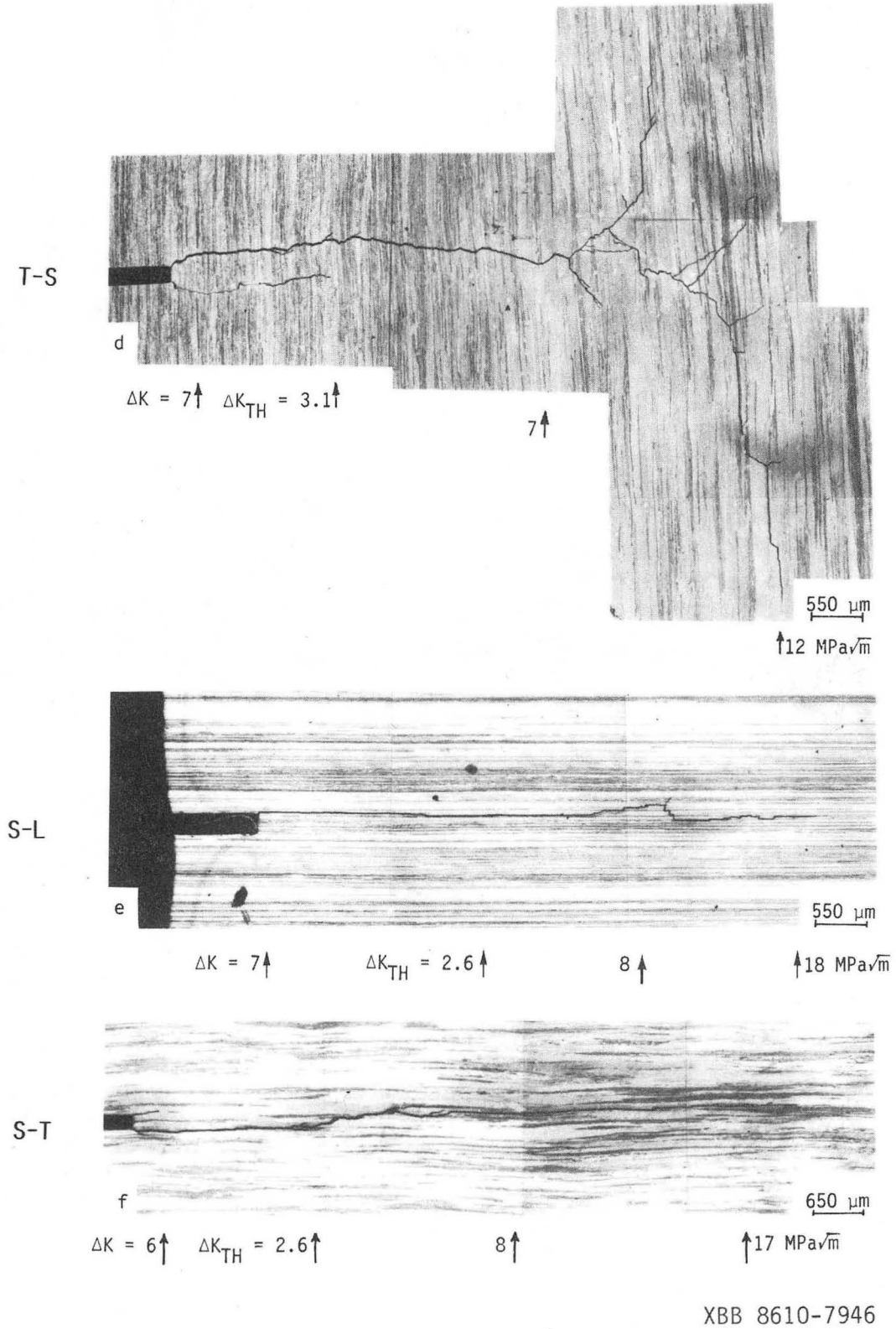
T-S
d
ΔK = 7↑ ΔK$_{TH}$ = 3.1↑
7↑
550 μm
↑12 MPa√m
S-L
e
550 μm
ΔK = 7↑ ΔK$_{TH}$ = 2.6↑ 8↑ ↑18 MPa√m
S-T
f
650 μm
ΔK = 6↑ ΔK$_{TH}$ = 2.6↑ 8↑ ↑17 MPa√m
XBB 8610-7946

Fig. 11 (Cont.)

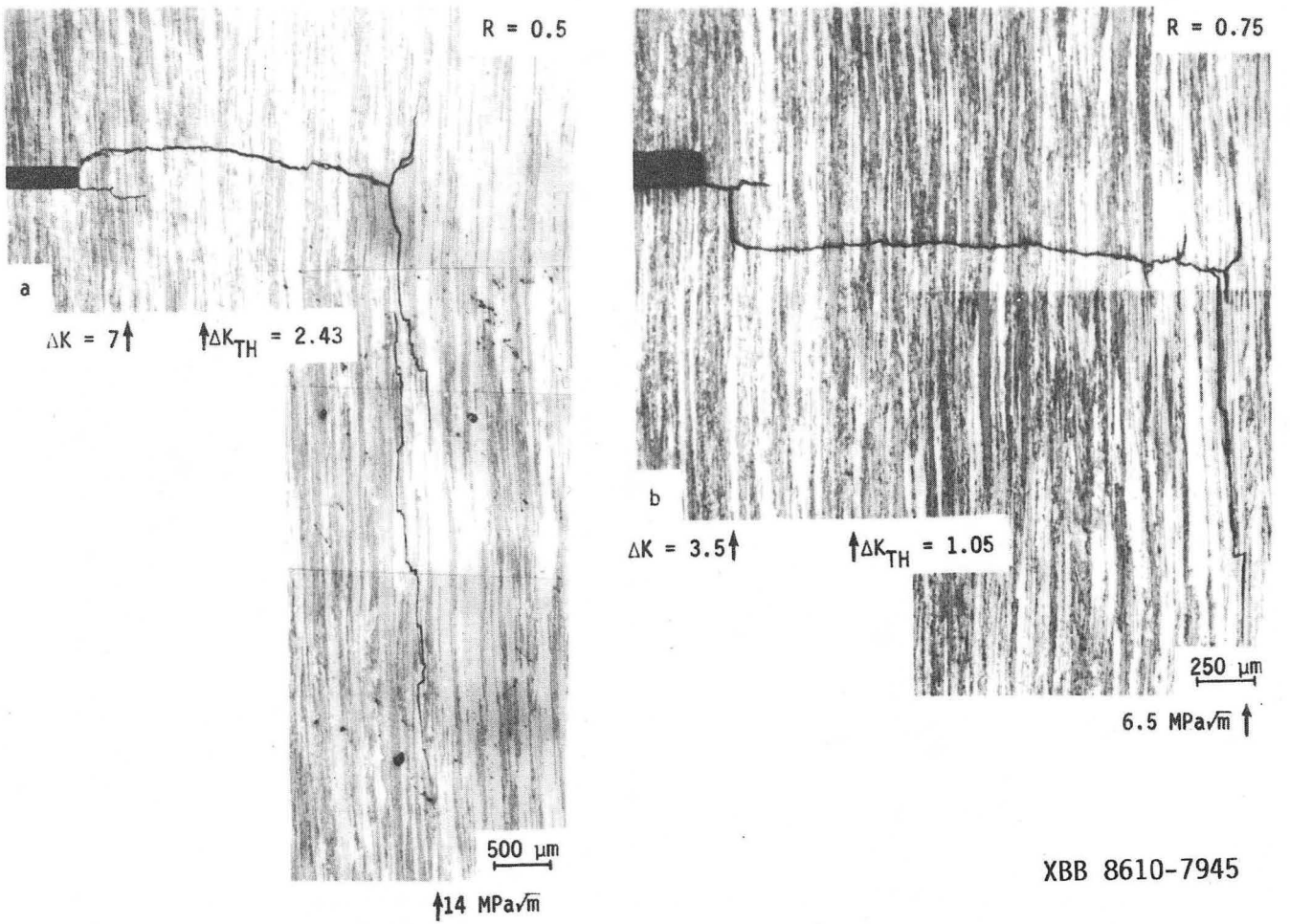

Fig. 12: Crack path profiles for the T-S orientation in 2090-T8E41 alloy at a) R = 0.5, and b) R = 0.75, showing macroscopic 90° branching of the crack along the rolling plane (parallel to the tensile stress axis).

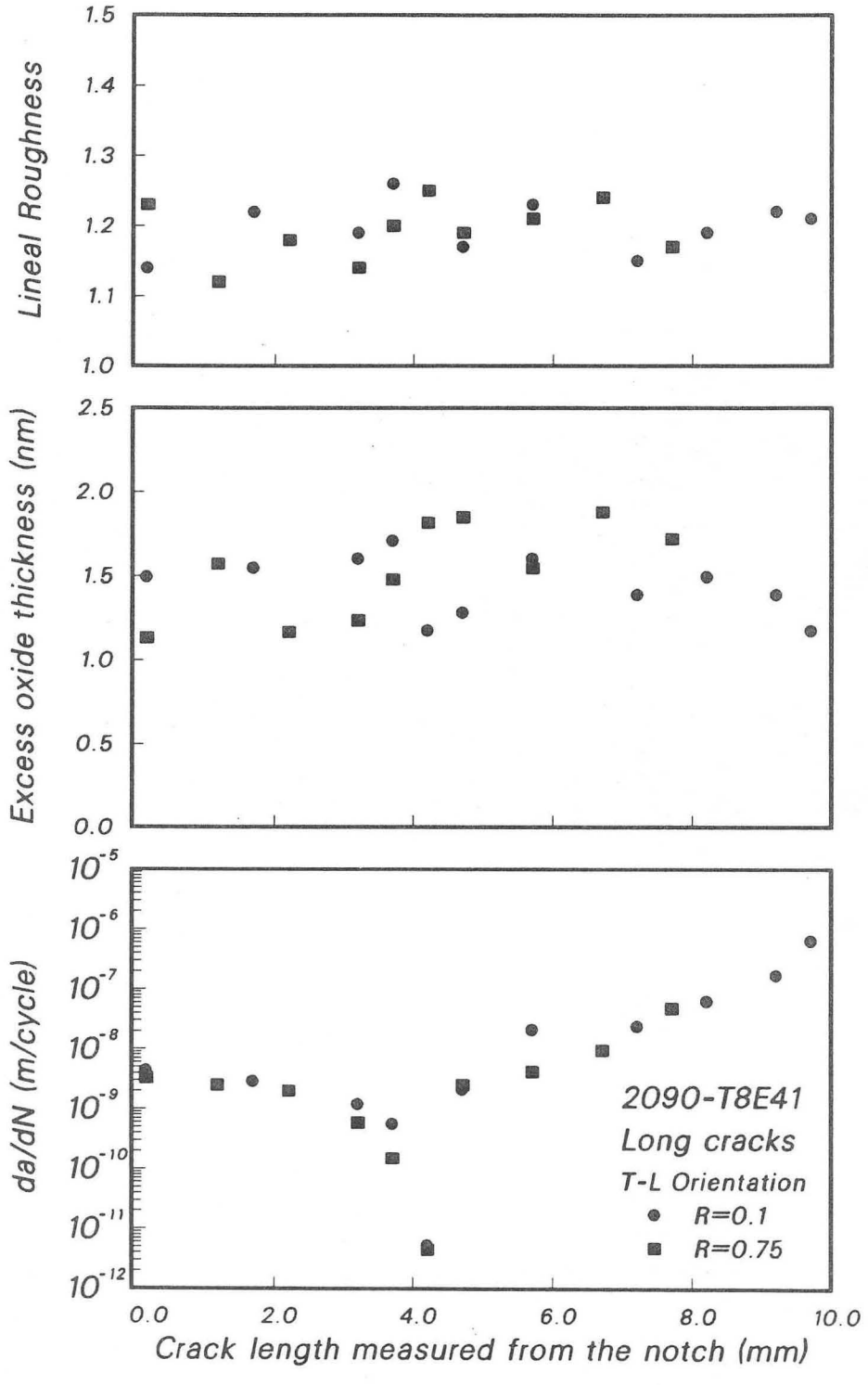

Fig. 13: Variation in a) crack surface excess oxide thickness, b) fracture surface lineal roughness, and c) crack growth rate, with crack length (measured from notch) for fatigue crack extension in 2090-T8E41 alloy. Data obtained for T-L orientation at R = 0.1 and 0.75.

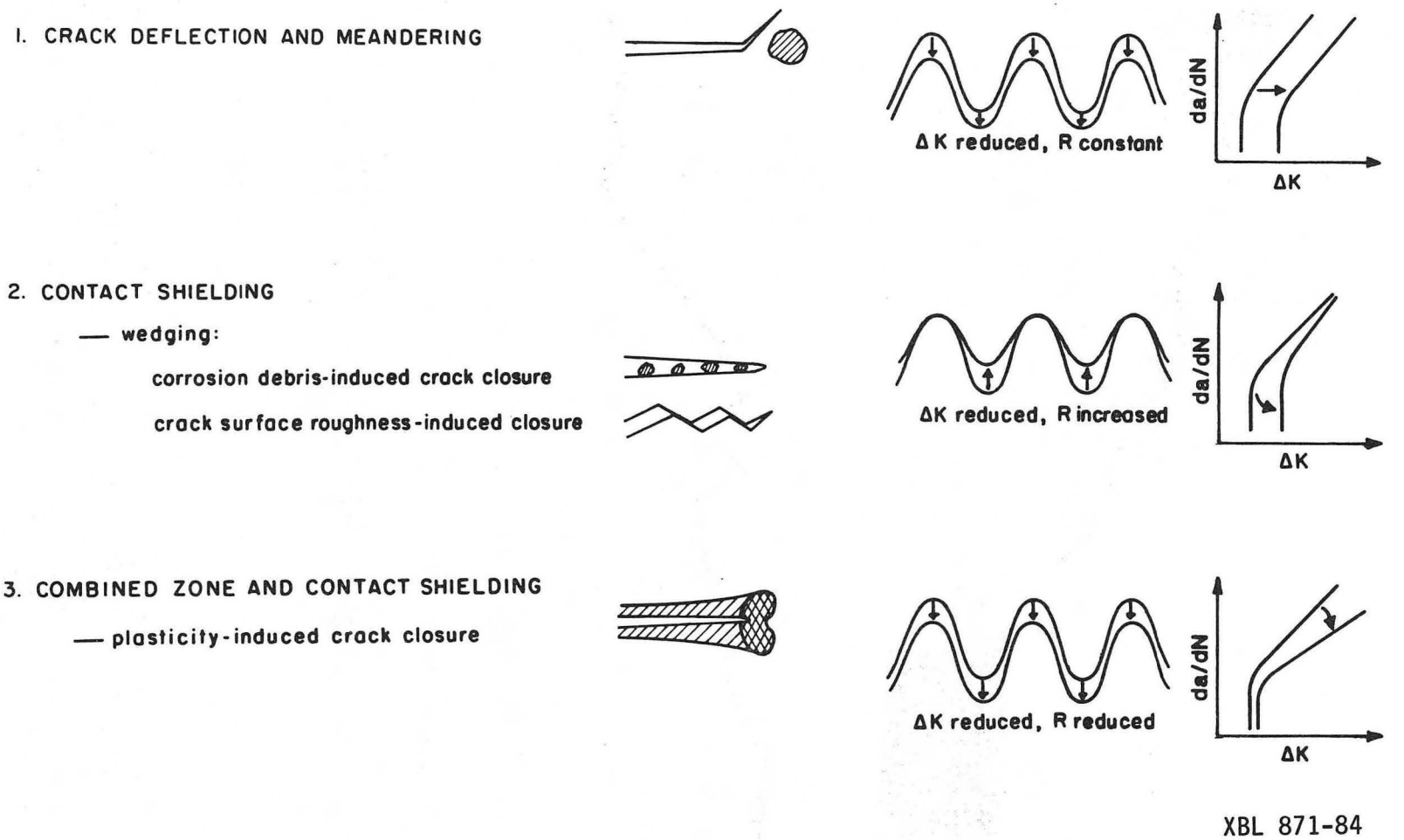

Fig. 14. Schematic illustration of crack tip shielding in aluminum-lithium alloy 2090-T8E41, showing primary mechanisms and their consequences to crack growth behavior.

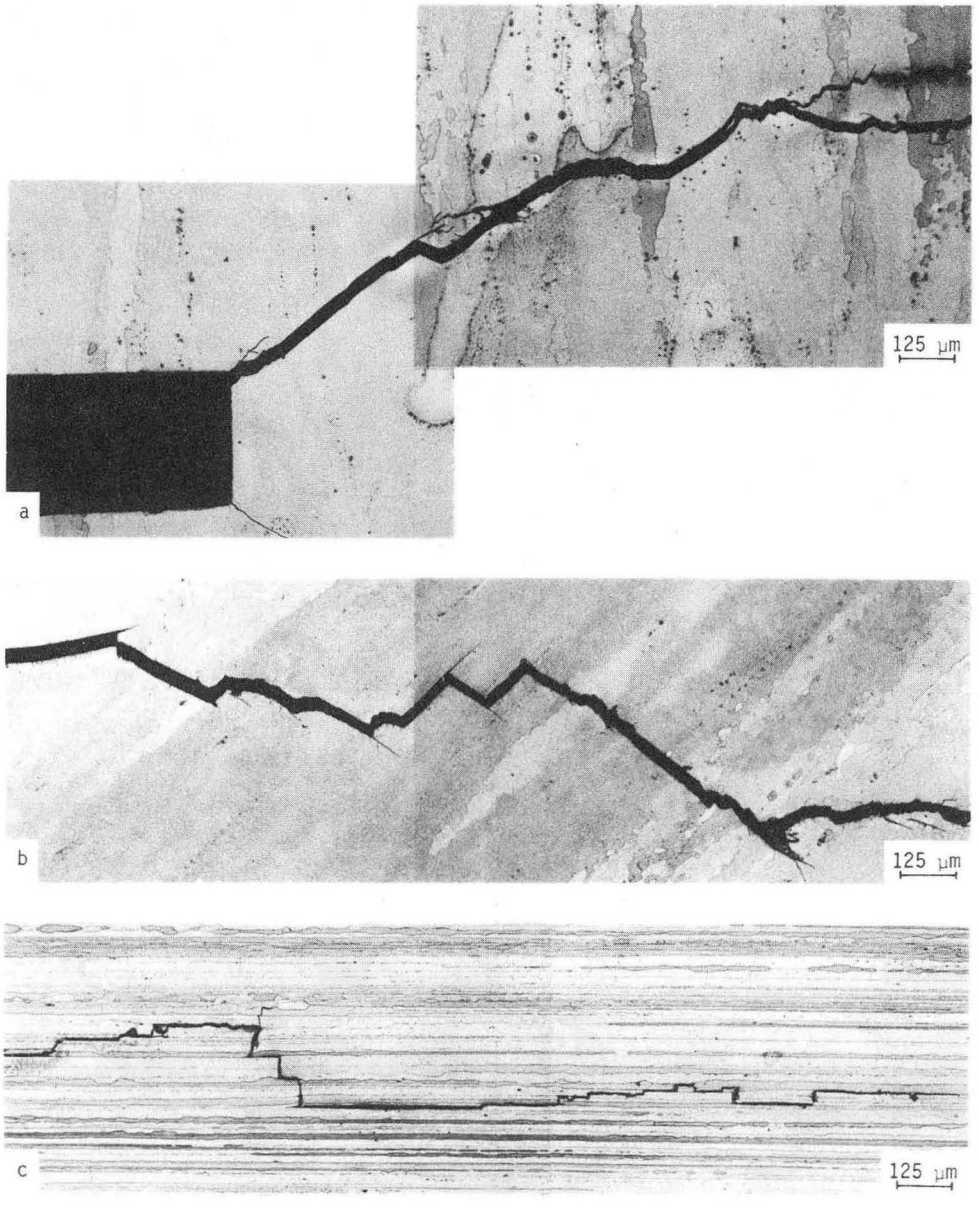

XBB 869-7356

Fig. 15: Types of crack path meandering during fatigue crack propagation in 2090-T8E41 alloy, showing a) macroscopic crack branching in the L-T orientation, b) microscopic crack deflection (crystallographic slip-band cracking) in L+45 orientation, and c) intergranular delamination-type cracking in S-L orientation.

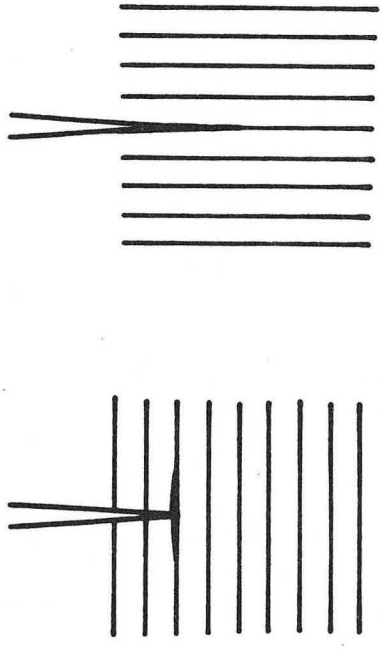

XBL 871-359

Fig. 16: Schematic representation of crack extension perpendicular and parallel to the weak layers normal to the short-transverse direction (in the rolling plane).

This report was done with support from the Department of Energy. Any conclusions or opinions expressed in this report represent solely those of the author(s) and not necessarily those of The Regents of the University of California, the Lawrence Berkeley Laboratory or the Department of Energy.

Reference to a company or product name does not imply approval or recommendation of the product by the University of California or the U.S. Department of Energy to the exclusion of others that may be suitable.

LAWRENCE BERKELEY LABORATORY
TECHNICAL INFORMATION DEPARTMENT
UNIVERSITY OF CALIFORNIA
BERKELEY, CALIFORNIA 94720